Study on the condensation pattern of steam jet under different back pressure conditions

An Cao[a], Xinxing Liu[b], Yongzhen Hua[c], Zhaoming Meng[a,*], Guangming Fan[a]

[a] Heilongjiang Provincial Key Laboratory of Nuclear Power System & Equipment, Harbin Engineering University, Harbin 150001, PR China

[b]Bohai Shipyard Co., Ltd, Huludao 125004, PR China

[c] China Nuclear Power Engineering Co., Ltd, Beijing 100840, PR China

Abstract: In the practical application of engineering, the phenomenon of steam underwater immersion jet under high back pressure conditions (>0.1MPa) exists. However, most of the current research on steam immersion jet condensation flow patterns and their boundaries is conducted under atmospheric pressure conditions (0.1MPa). The applicability of condensation flow patterns and related prediction formulas derived under atmospheric pressure to high back pressure conditions remains to be validated. Based on the experimental research, the condensation pattern of steam underwater immersion jet under different back pressure conditions is identified, and the condensation behavior of the jet under different back pressure conditions is clarified by comparing and analyzing the visual images and dynamic pressure characteristics of different condensation flow patterns, and the influence law of back pressure and other parameters on the condensation flow pattern boundary is mastered. This study fills the gap in the research of steam underwater immersion jet under the condition of high back pressure, which has important scientific research significance and engineering application value.

Keywords: Steam Immersion Jet; Condensation Flow Pattern; Flow Pattern Boundary; Back Pressure; Dynamic Pressure Characteristics

1. INTRODUCTION

The vapor-liquid interface structure of the steam underwater immersion jet is affected by the coupling of flow and heat transfer processes, and the accurate identification and classification of the vapor-liquid interface structure is the basis for the study of steam jet characteristics [1-6].

Under the condition that the back pressure of the pool is atmospheric pressure（0.1MPa）, Arinobu [7] divided the condensate flow pattern into six regions （I-VII） by observing the structure of the vapor-liquid interface and the measured pressure oscillation characteristics. In region I, due to the small mass flow rate of steam and the high supercooling degree of pool water, the steam is completely condensed in the nozzle, and the steam-liquid interface oscillates in the nozzle, and there is a coupling relationship between the pressure oscillation and the interface oscillation. In Zone II, steam intermittently enters the pool from the nozzle, a process accompanied by the back-up of the pool water. In Zone VI, the condensation is further weakened, the bubble volume becomes larger, and some of the steam cannot be condensed and escape from the water surface.

Chan and Lee [8] carried out similar experiments using a nozzle with a larger nozzle diameter, and they divided the flow pattern into bubble-wrapped chugging and bubble-detached chugging according to the position of the steam mass flow velocity below 80 kg/(m^2·s). Under the condition that the steam mass flow velocity is higher than 80 kg/(m^2·s), it is divided into ellipsoidal bubble, ellipsoidal jet and conical jet according to the shape of the steam cavity.

* Corresponding author.

Name: Zhaoming Meng. Complete address: No. 145, Nantong Street, Nangang District, Harbin City. Telephone number: 13258671861. E-mail addresses: mengzhaoming@hrbeu.edu.cn.

In the flow pattern given by Nariai and Aya [9], the boundaries of the chugging flow pattern are in good agreement with those in the Arinobu [7] flow pattern, but there are some differences between the boundaries of other flow patterns. Cho et al. [10] identified six condensation flow patterns in a wide range of steam mass flow velocities, namely chugging flow pattern, transient chugging flow pattern, condensation oscillation flow pattern, bubbling condensation oscillation flow pattern, stable condensation flow pattern, and interface oscillation condensation flow pattern. The transient chugging flow pattern is similar to the phenomenon observed in the Nariai and Aya [9] experiments, and the transient chugging flow pattern is called a small chugging in the flow pattern diagram of Nariai and Aya [9].

Most of the scholars' condensation pattern diagrams are based on the experimental datas of the open pool, and the back pressure of the pool is maintained at the atmospheric environmental pressure, and a few scholars have carried out relevant studies on the condensation pattern under non-atmospheric pressure conditions. Among them, Mazed et al. [11] studied the condensation behavior of the steam jet under the condition that the back pressure of the pressure suppression box is 17.01~27.22 kPa (absolute pressure) in the context of the vacuum chamber overpressure protection system in the International Thermonuclear Experimental Reactor, and established the condensation flow pattern in a small steam mass velocity range, but the chugging flow pattern was not found, which may be due to the change of the supercooling degree of the pool and the flow rate of the steam outlet after the pressure suppression pool was vacuumed. This in turn affects the condensation process of the steam jet. Lee et al. [12] also used a closed pool to simulate a core make-up tank (CMT) to study the jet condensation process that occurs when a large amount of steam is introduced into the CMT from the regulator's pressure balance line during the loss of coolant accident (LOCA). Although they established the corresponding flow pattern, the back pressure was increasing during the experiment, and the effect of back pressure on the condensation flow pattern was not explained.

In view of the large differences between the condensation flow patterns established by different scholars, Zhao and Hibiki [13] redefined many different condensate flow patterns according to the flow pattern characteristics, and summarized them as chugging flow patterns, hemispherical bubble oscillation flow patterns, condensation oscillation flow patterns, stable condensation flow patterns, and incomplete condensation flow patterns, but the result is that there are still large differences between the condensation flow patterns of different scholars. Based on this, it may be that the definition of the condensate pattern boundary is too subjective, or that the condensate pattern conversion is affected by a combination of factors.

Liang and Griffith [14] took whether the pool water enters the nozzle as the critical point of chugging occurrence, and made a variety of ideal assumptions about the process, and derived the judgment criterion for chugging occurrence based on the principle of conservation of mass and energy, but compared with the experimental data, it was found that the deviation between the predicted value and the experimental value was too large when the supercooling degree was low. Based on the balance between the amount of steam supplied and the amount of condensation passing through the bubble surface, they deduced the boundary between the condensing oscillatory flow pattern and the stable condensation flow pattern. It should be pointed out that the derivation process of Liang and Griffith [14] is based on the vertical upward jet condensation process of steam in co-directional flowing water, and it remains to be verified whether the condensation of steam jet under other conditions needs to be verified.

In summary, most of the existing studies on steam jet condensation modes and flow pattern boundaries are carried out under the condition that the back pressure is atmospheric pressure, and there is a lack of research under the condition of high back pressure [15-20]. Therefore, in this study, an experimental setup for steam jet under high back pressure conditions is built, and the condensation patterns of steam underwater

immersion jets under different back pressure conditions are studied and identified, and the visualization images and dynamic pressure characteristics of different condensation patterns are compared and analyzed, and the influence of parameters such as back pressure and nozzle diameter on the boundary of condensate flow patterns is mastered.

2. EXPERIMENTAL SETUP

The experimental setup is shown in Fig. 2.1. It is mainly composed of six parts: steam supply system, visual pressure pool, nozzle assembly, pool water level adjustment system, pool back pressure control system and data measurement and acquisition system [21-23].

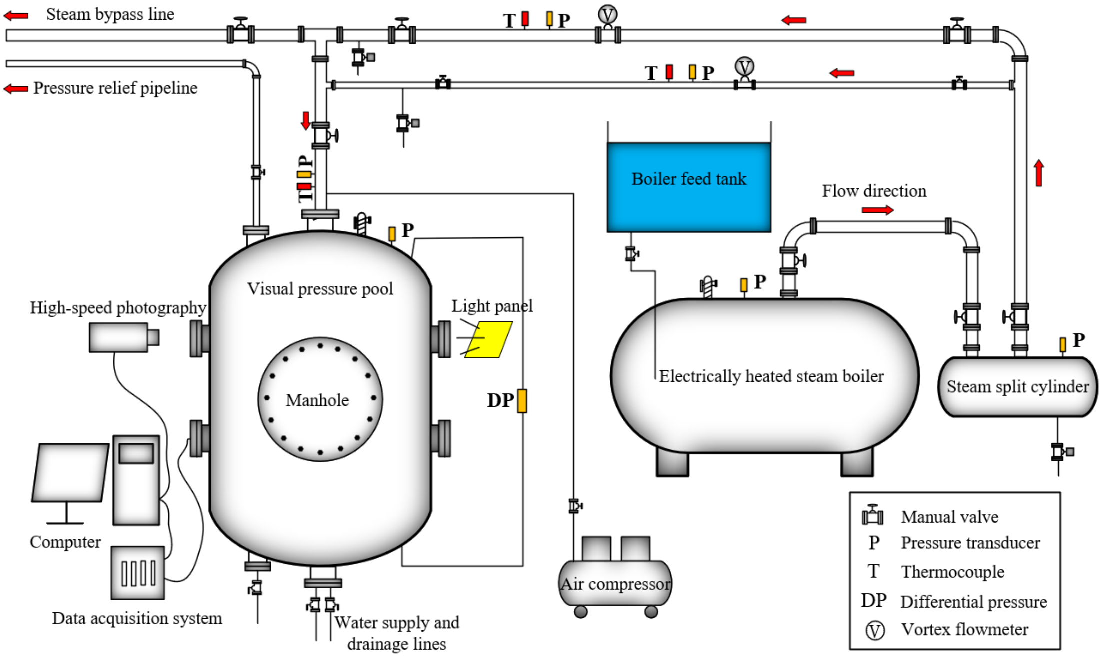

Fig. 2.1 Schematic diagram of the experimental setup

The steam supply system provides saturated steam to meet the conditions required for the experiment. The steam used in the experiment is produced by an electrically heated steam boiler and fed into a pool through steam pipes and valves. The electrically heated steam boiler has a rated power of 700 kW and a rated steam production capacity of 1000 kg/h, and can supply saturated steam with a rated pressure of 1 MPa.

The visual pressure pool is used to simulate the environment of the suppressed pool under different back pressure conditions. The visual pressure pool is made of 304 stainless steel, with a maximum pressure of 1 MPa, and a safety valve is set at the top to prevent overpressure. The wall thickness of the pool is 8 mm, the inner diameter is 1200 mm, and the height is 2000 mm. A manhole with a diameter of 500 mm is reserved on the side of the pool to facilitate personnel to enter and exit the installation and maintenance of related measuring instruments. Quartz glass windows with a diameter of 200 mm are reserved at the upper part of the surface of the side wall of the pool for visualization of high-speed photography and background light source arrangement in the experiment.

The nozzle assembly is used to investigate the effect of the nozzle diameter on the condensation characteristics of the jet. The nozzle assembly consists of two stainless steel nozzles in different sizes, with an inner diameter of 28 mm and 38 mm. The wall thickness of the 28 mm diameter nozzle is 2 mm, and the wall thickness of the 38 mm diameter nozzle is 38 mm. Each nozzle has a length of 650 mm. The outlet of the nozzle is vertically downward along the central axis of the pressure pool, the outlet is 1250 mm from the bottom of the pool, and the inlet is connected with the steam pipe by a flange for easy replacement. The outlet immersion depth of the

nozzle is 300 mm.

The water level control system is used to fill and drain the pool before and after the experiment and to maintain the required water level during the experiment. The water level control system consists of visualizing the water supply and drainage lines at the bottom of the pool and the overflow line inside the pool. In the preparation phase of the experiment, the water inlet valve is opened and the initial water level is adjusted. During the experiment, the water level rose due to the continuous condensation of the steam entering the pool, and in order to keep the immersion depth of the nozzle constant, an overflow line as shown in Fig. 2.2 is designed inside the pool. In the atmospheric pressure test, the overflow line valve can be kept open to stabilize the water level, while under high back pressure conditions, the valve opening needs to be adjusted to maintain the water level under the condition of ensuring that the back pressure is stable. At the end of the experiment, the water in the pressure pool can be drained through the drain valve.

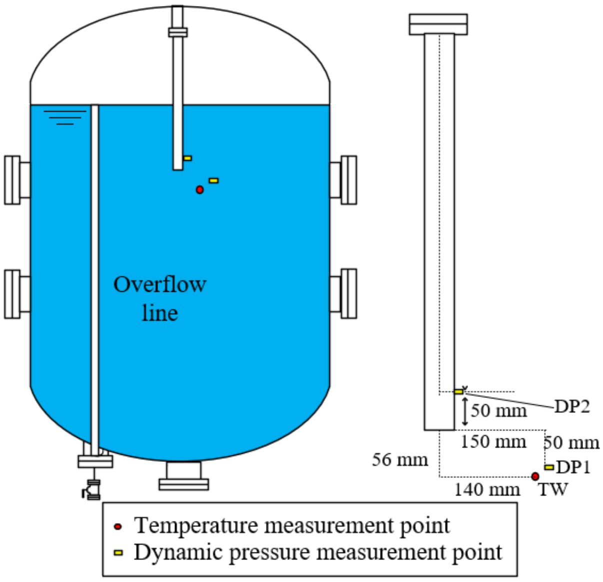

Fig. 2.2 Schematic diagram of measuring point position

The back pressure control system is used to provide a stable back pressure environment for the pool. The air generated by the air compressor enters the visual pressure pool through the steam inlet pipeline for pressurization. The pressure is relieved by the pressure relief pipeline connecting the pool gas space and the external environment. The two work together to adjust the back pressure to reach the preset initial value of the experiment. In the process of atmospheric pressure test, the stable back pressure of the pool can be maintained by keeping the pressure relief pipeline valve normally open, and in the process of high back pressure test, the change of back pressure can be monitored through the data measurement and acquisition system, so as to manually adjust the opening of the pressure relief pipeline valve, so that the back pressure environment of the pool can be kept fluctuating within a certain range.

Data measurement and acquisition system is used to measure, monitor and record relevant experimental datas. A flowmeter is installed on the steam pipeline to measure the steam volume flow, and a pressure sensor and a thermocouple are installed at the specified position downstream of the flowmeter for temperature and pressure compensation for the measured steam flow. A thermocouple is arranged near the nozzle nozzle for measuring the water temperature of the pool, and a high-frequency dynamic pressure sensor is installed in the nozzle and in the pool respectively, which is used for measuring the dynamic pressure generated by the condensation of the steam jet, and the specific measuring point position is shown in Fig. 2.2. Temperature, pressure, and steam volume flow data are monitored and recorded with an NI data acquisition system at a

sampling frequency of 20 Hz. The dynamic pressure sampling frequency is set to 20 kHz, and the sampling time is 20 s.

The parameters of the measuring instrument and the uncertainty of the parameters are shown in Table 2.1. The experimental conditions are shown in Table 2.2.

Table 2.1 Measurement instrument parameters and parameter uncertainty

Measuring instruments	Parameters	Range	Uncertainty
Vortex flowmeter	Steam volume flow rate	0~350 m^3/h	4.4%
T-type thermocouple	Temperature	-40~350℃	1.0%
Pressure transducer	Steam pressure Pool back pressure	0~1MPa	1.7%
Differential pressure transducer	Differential pressure	0~60kPa	3.2%
Dynamic pressure transducer	Dynamic pressure	0~3000kPa 0~500kPa	4%

Table 2.2 Experimental conditions

Pool back pressure (MPa, abs)	Nozzle inner diameter (mm)	Steam mass flow velocity [$kg/(m^2 \cdot s)$]	Water temperature (°C)
0.1	28	10, 15, 20, 25, 30, 40, 50, 60, 70, 80, 90	20~95
0.1	38	15, 20, 30, 40, 50, 60	20~95
0.2	28	10, 15, 20, 25, 30, 40, 50, 60, 70, 80, 90	20~115
0.2	38	15, 20, 30, 40, 50, 60	20~115
0.25	28	60, 80	50~90
0.3	28	10, 15, 20, 30, 40, 50, 60, 70, 80, 90	20~128
0.3	38	50, 60	20~128
0.4	28	20, 30, 40, 50, 60, 70, 80, 90	20~138

3. RESULTS AND DISCUSSION

3.1 Steam jet condensation flow pattern

Within the experimental parameters studied, four different condensation patterns are observed, which are named chugging, non-periodic condensation oscillation, periodic condensation oscillation and bubbling condensation according to their different phase interface characteristics and dynamic pressure characteristics, respectively. In order to visually demonstrate the influence of parameters such as steam mass flow velocity, water temperature, nozzle diameter and back pressure on the condensate flow pattern partition, the condensate flow pattern of steam jet as shown in Fig. 3.1 and Fig. 3.2 is plotted.

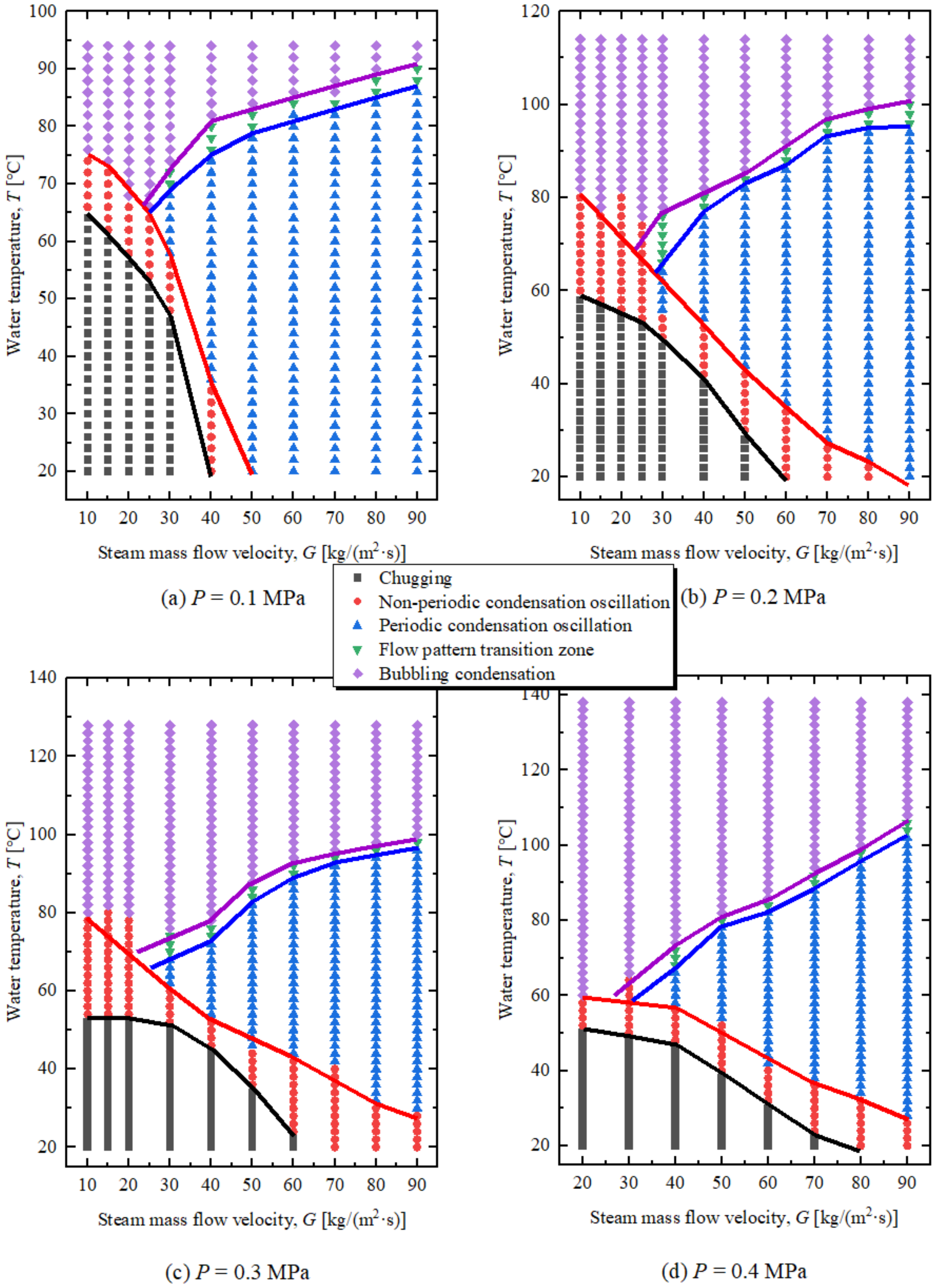

Fig. 3.1 Condensation regime maps for different ambient pressures (D = 28 mm)

The abscissa and ordinate of the condensate flow pattern are the steam mass flow velocity and water temperature, respectively, and the chugging flow pattern is located in the lower left corner of the condensate flow pattern, corresponding to the lower steam mass flow velocity and water temperature. Chugging usually occurs when the water temperature is lower than 65 °C, and the water temperature corresponding to the upper boundary of the chugging flow pattern decreases gradually with the increase of steam mass flow velocity. As shown in Fig. 3.1 (a), the flow pattern changes from chugging to non-periodic condensation oscillation at about 65 °C when the steam mass flow velocity is 10 kg/(m^2·s), and decreases to about 47 °C when the steam mass flow velocity increases to 30 kg/(m^2·s), and the chugging

disappears completely when the steam mass flow velocity is further increased to 40 kg/(m^2·s), and the same change pattern is observed under other higher back pressure conditions. Comparing the distribution of chugging flow patterns under different back pressure conditions in Fig. 3.1, it can be seen that when the back pressure increases from 0.1 MPa to 0.4 MPa, the steam mass flow velocity needs to increase from 40 kg/(m^2·s) to 80 kg/(m^2·s) before the chugging phenomenon no longer occurs.

After the water temperature reaches the corresponding temperature at the upper boundary of the chugging flow pattern region, the flow pattern changes to a non-periodic condensation oscillation if the temperature continues to rise. The non-periodic condensation oscillation can occur under the condition of different steam mass flow velocities, while the periodic condensation oscillation only occurs under the condition that the steam mass flow velocity reaches 30 kg/(m^2·s) and above, and with the increase of steam mass flow velocity, the water temperature corresponding to the upper boundary of the periodic condensation oscillation gradually increases, and the corresponding water temperature corresponding to the lower boundary gradually decreases, covering a larger range of water temperature. Similar to the effect of back pressure on chugging flow pattern, under atmospheric pressure conditions, when the steam mass flow velocity reaches 50 kg/(m^2·s), the non-periodic condensation oscillation phenomenon disappears, but with the increase of back pressure to 0.4 MPa, the non-periodic condensation oscillation phenomenon still occurs even under the maximum steam mass flow velocity.

There is a transition zone with a temperature variation range of about 2~6 °C at the upper boundary of the periodic condensation oscillation zone, and it enters the bubbling condensation zone after crossing this zone. Bubbling condensation usually starts when the water temperature reaches about 70~80 °C, and lasts until the water temperature is close to saturation and begins to appear incomplete condensation of steam.

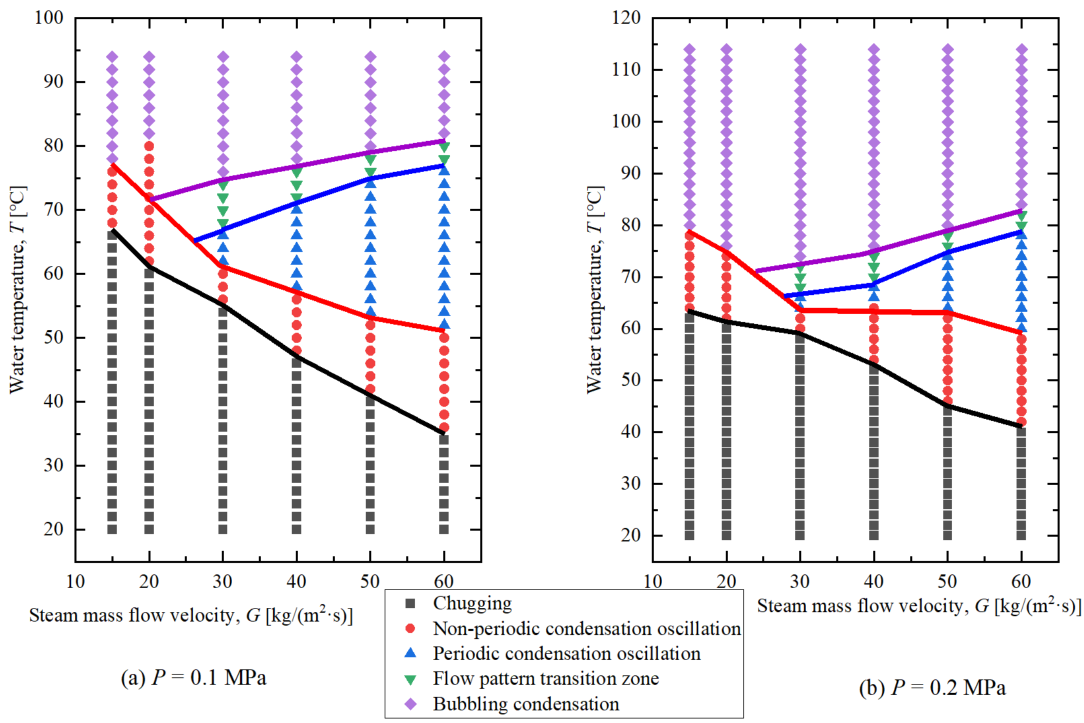

Fig. 3.2 Condensation regime maps for different ambient pressures (D = 38 mm)

These four flow patterns are also observed in the flow pattern diagram for larger nozzle diameters shown in Fig. 3.2, but as the nozzle diameter increases, the range of the chugging flow pattern in the flow pattern increases, while the coverage of the periodic condensation oscillation flow pattern

decreases accordingly.

3.2 Characteristics of jet condensation pattern

3.2.1 Chugging flow pattern

The hallmark feature of the chugging phenomenon is that the pool water is intermittently sucked in and ejected from the nozzle. As shown in Fig. 3.3 (a), at 0 ms, the steam enters the pool from the nozzle outlet to form a bubble, which gradually expands and reaches its maximum volume at about 300 ms, followed by an upward motion under buoyancy that envelops the nozzle mouth. Due to the low temperature of the pool water and the strong condensation ability when the chugging occurs, the bubble quickly condenses and collapses within 5 ms, producing a huge "bang" sound and forming a negative pressure in the nozzle. As a result, under the action of the pressure difference between the inside and outside of the nozzle, the pool water began to be sucked into the nozzle at 405 ms. The pool water entering the nozzle is continuously heated by steam, and the condensation gradually weakens. At the same time, the accumulation of steam in the nozzle causes the pressure in the nozzle to rise, causing the pool water entering the nozzle to remain in the nozzle for a period of time and then be pushed out of the nozzle (1445 ms), and then the steam expands at the nozzle mouth to form a new bubble and circulate the process.

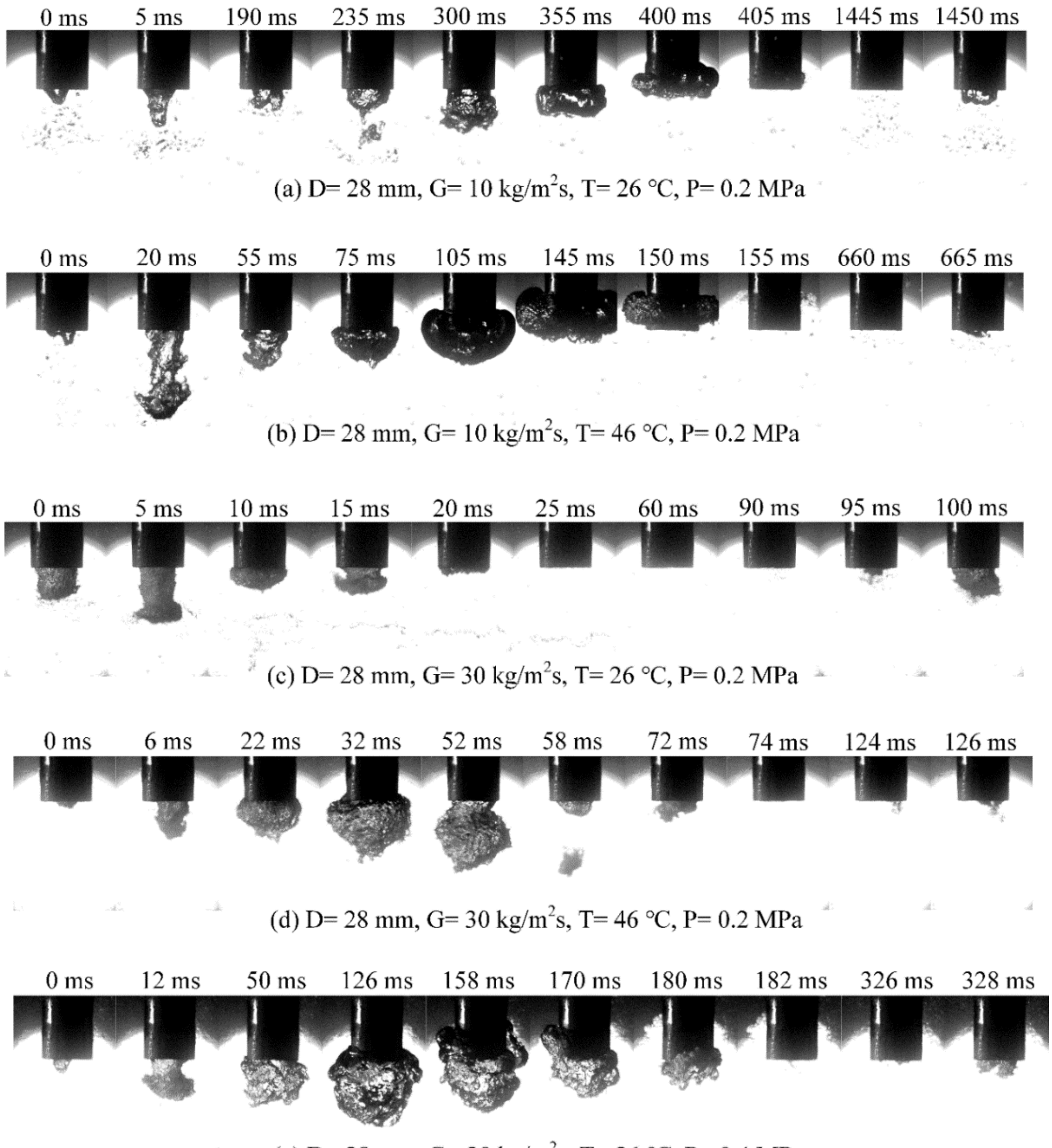

(a) D= 28 mm, G= 10 kg/m^{2}s, T= 26 °C, P= 0.2 MPa

(b) D= 28 mm, G= 10 kg/m^{2}s, T= 46 °C, P= 0.2 MPa

(c) D= 28 mm, G= 30 kg/m^{2}s, T= 26 °C, P= 0.2 MPa

(d) D= 28 mm, G= 30 kg/m^{2}s, T= 46 °C, P= 0.2 MPa

(e) D= 28 mm, G= 30 kg/m^{2}s, T= 26 °C, P= 0.4 MPa

Fig. 3.3 Interface evolutions of chugging

Comparing the interface change images in Fig. 3.3 (a)~(d), it can be seen that the maximum volume of bubbles that can expand increases when the water temperature increases, and the residence time of the pool water in the nozzle is shortened, and the retention time in the pool water nozzle can be shortened by increasing the steam mass flow velocity. Fig. 3.3 (c) and (e) show that when the back pressure increases, the maximum volume of bubbles increases, and the retention time of the pool water in the nozzle also increases from 70 ms to about 140 ms.

In the experiment, two bubble morphologies under the chugging flow pattern are observed, one is the downward growth type and the other is the upward envelope type, which generally appeared in the early and late stages of bubble growth, respectively. When the water temperature rises, the bubble becomes larger and more buoyant, and the maximum distance that can be reached by the upward envelope bubble increases from only at the outlet of the nozzle to about double the nozzle diameter. As shown in Fig. 3.3 (c), when the steam mass flow velocity increases to 30 kg/(m^2·s), the inertial force on the bubble is greater, and the upward envelope bubble no longer appears. On this basis, increasing the back pressure will reduce the flow rate at the outlet of the bubble, and the upward envelope bubble will reappear.

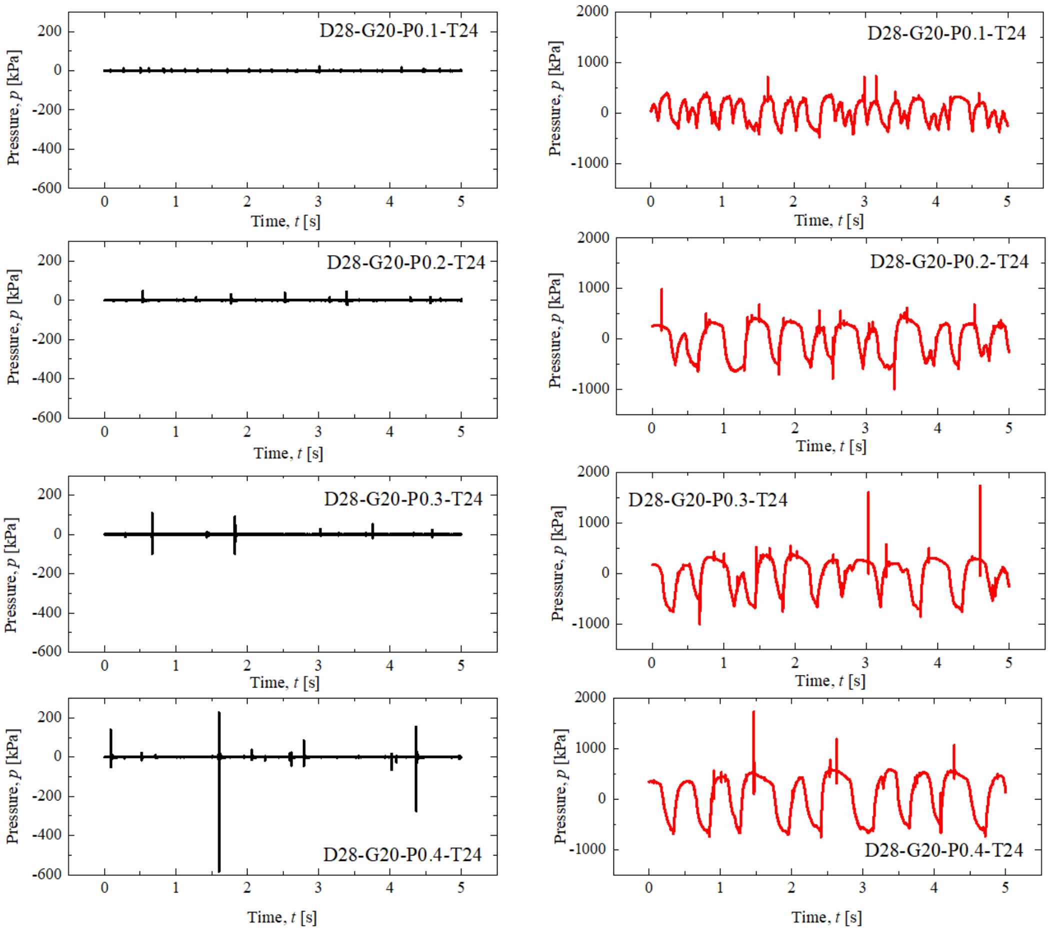

(a) Dynamic pressure in the pool (b) Dynamic pressure in the nozzle

Fig. 3.4 Dynamic pressure of chugging

The dynamic pressure changes in the pool and in the nozzle measured under the chugging flow pattern are shown in Fig. 3.4. In the chugging flow pattern, the vapor-liquid interface intermittently moves in and out of the nozzle. When the vapor-liquid interface is outside the nozzle, the instantaneous condensation of the bubble at the nozzle will produce a strong pressure pulse in the pool, and when the vapor-liquid interface oscillates up and down in the nozzle, the pool water at the nozzle is sucked in or sprayed out,

and the pressure fluctuation caused in the pool is small, so the dynamic pressure change in the pool presents the characteristics of weak fluctuations and multiple sharp peaks as shown in Fig. 3.4. Since positive and negative pressures are alternately formed in the nozzle during the chugging process, the dynamic pressure measured in the nozzle shows the characteristics of fluctuating up and down in a form similar to a sine wave, with a frequency of about 1~4 Hz and an amplitude of hundreds of kPa. On the basis of this large pressure fluctuation at low frequencies, megapascal pressure pulses also occur, which are caused by condensation-induced water hammer caused by the backflow of pool water after the rapid condensation of the steam in the nozzle [24, 25].

In Fig. 3.4, D, G, P, and T represent nozzle diameter, steam mass flow velocity, back pressure, and water temperature, respectively, and the same is true for the following paragraphs. In Fig. 3.4, the steam mass flow velocity and water temperature conditions are the same from top to bottom, but the back pressure increases sequentially. It can be seen that the peak pressure pulse in the pool increases from less than 20 kPa to more than 200 kPa with the increase of back pressure. In the nozzle, the pressure fluctuation amplitude accompanied by the oscillation of the vapor-liquid interface increased from about 400 kPa at a back pressure of 0.1 MPa to 600 kPa at a back pressure of 0.4 MPa, and the peak value of the pressure pulse caused by condensation-induced water hammer also increased from about 700 kPa to about 1700 kPa with the increase of back pressure. The frequency of pressure fluctuations tends to decrease with the increase of back pressure.

3.2.2 Non-periodic condensation oscillation flow pattern

On the basis of the chugging flow pattern, when the water temperature continues to rise, the condensation ability of the pool water is weakened, the phenomenon of instantaneous collapse of the whole bubble will no longer occur, and the pool water will not enter the nozzle, and the condensation flow type will be converted to non-periodic condensation oscillation. As shown in Fig. 3.5, the bubble gradually expands to a certain volume at the outlet of the nozzle and then " necking", that is, it begins to shrink in the middle of the bubble, and then the lower half of the bubble breaks away from the original bubble, moves downward under the action of inertial force, and condenses and annihilates in a few milliseconds, and the surrounding water body quickly fills the space occupied by the bubble, and the impact produces a sound, while the upper bubble continues to expand and starts the next round of condensation and oscillation.

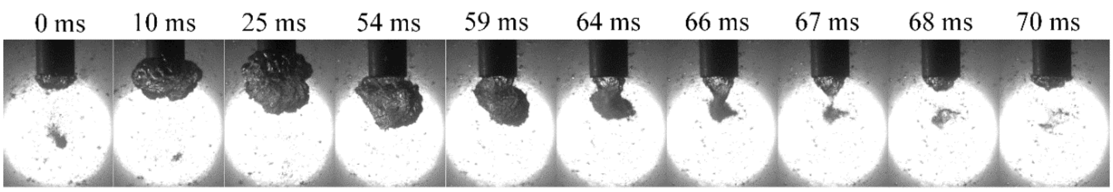

(a) D= 28 mm, G= 20 kg/m^{2}s, T= 58 °C, P= 0.1 MPa

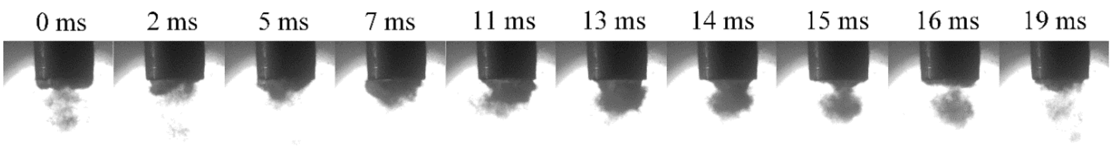

(b) D= 28 mm, G= 60 kg/m^{2}s, T= 30 °C, P= 0.2 MPa

Fig. 3.5 Interface evolutions of non-periodic condensation oscillation

The aperiodic condensation oscillation flow pattern is characterized by the irregularity of the occurrence time of condensation oscillation. Taking the case in Fig. 3.5(a) as an example, the maximum volume of bubble expansion and the time interval between two adjacent condensation oscillation when

ten consecutive condensation oscillation occur are shown (Fig. 3.6). It can be seen that the maximum volume of the bubble varies significantly, and the time interval between condensation oscillation varies from a minimum of 11 ms to a maximum of 262 ms, which is completely random, and no obvious periodicity is found.

When the non-periodic condensation oscillation occurs, the "necking" of the bubbles at the nozzle also creates a pressure pulse in the pool, but the condensation rate is lower than the instantaneous condensation of the bubbles in the chugging flow pattern, so the pressure pulse value is smaller. As shown in Fig. 3.7, due to the random nature of the non-periodic condensation oscillation, the time intervals between two adjacent dynamic pressure peaks are also varied.

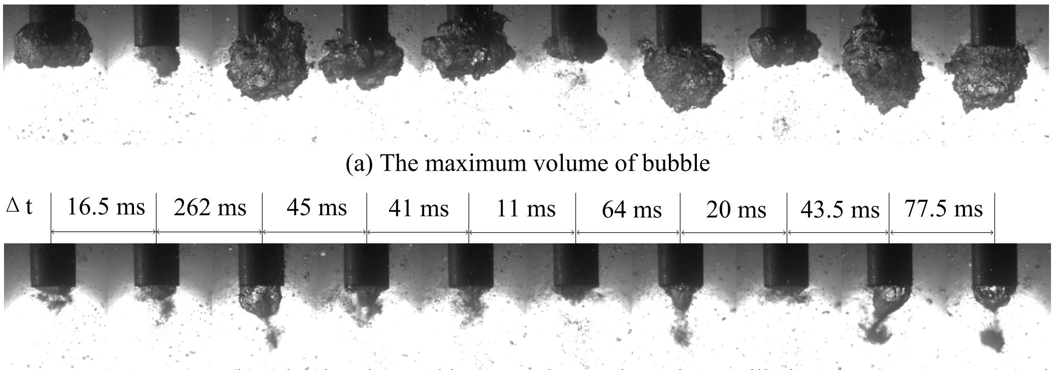

(b) The time interval between the condensation oscillation

Fig. 3.6 The images of the occurrence of non-periodic condensation oscillation [D = 28 mm, G = 20 kg/(m^2·s), T = 58 °C, P = 0.1 MPa)

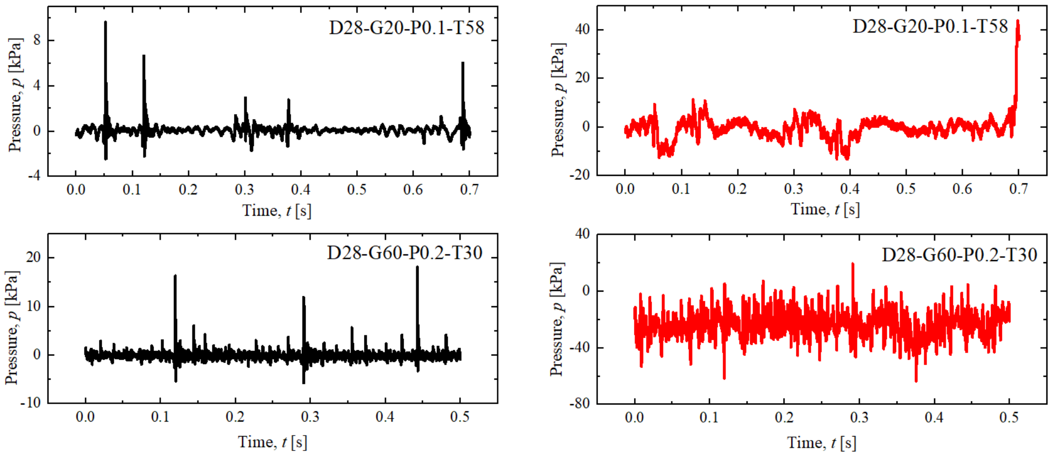

(a) Dynamic pressure in the pool (b) Dynamic pressure in the nozzle

Fig. 3.7 Dynamic pressure of non-periodic condensation oscillation

3.2.3 Periodic condensation oscillation flow pattern

As shown in Fig. 3.8, when the steam mass flow velocity increases above about 30 kg/(m^2·s), a "necking" phenomenon with the same characteristics as non-periodic condensation oscillation occurs. Fig. 3.9 shows the maximum volume of the bubble expanding to when ten consecutive condensation oscillation occur under this flow pattern and the time interval between the occurrence of two adjacent condensation oscillation, it can be seen that unlike the non-periodic condensation oscillation, the maximum volume that the bubble can reach is not much different, and the time interval between the condensation oscillation is mostly between 25 ms and 35 ms, which has obvious periodicity, so this flow pattern is called periodic condensation oscillation.

Fig. 3.8 illustrates the phase interface variation of periodic condensation oscillation flow patterns under different steam mass flow velocities, water

temperatures, and back pressure conditions over a complete period. Comparing Fig. 3.8 (a) and (c), it can be seen that the maximum volume of the bubble increases significantly when the water temperature rises from 56 °C to 86 °C under the same steam mass flow rate and the same back pressure, and the condensation oscillation period is obviously longer under the condition of high water temperature. As shown in Fig. 3.8 (c) and (d), the condensation oscillation period decreases from 11.5 ms to 7.5 ms as the steam mass flow rate increases from 60 kg/(m^2·s) to 90 kg/(m^2·s) under the same water temperature and the same back pressure. Fig.s 3.8 (b) and (c) show that the back pressure increases from 0.2 MPa to 0.4 MPa and the condensation oscillation period increases from 11.5 ms to 16.5 ms at the same steam mass flow rate and the same water temperature.

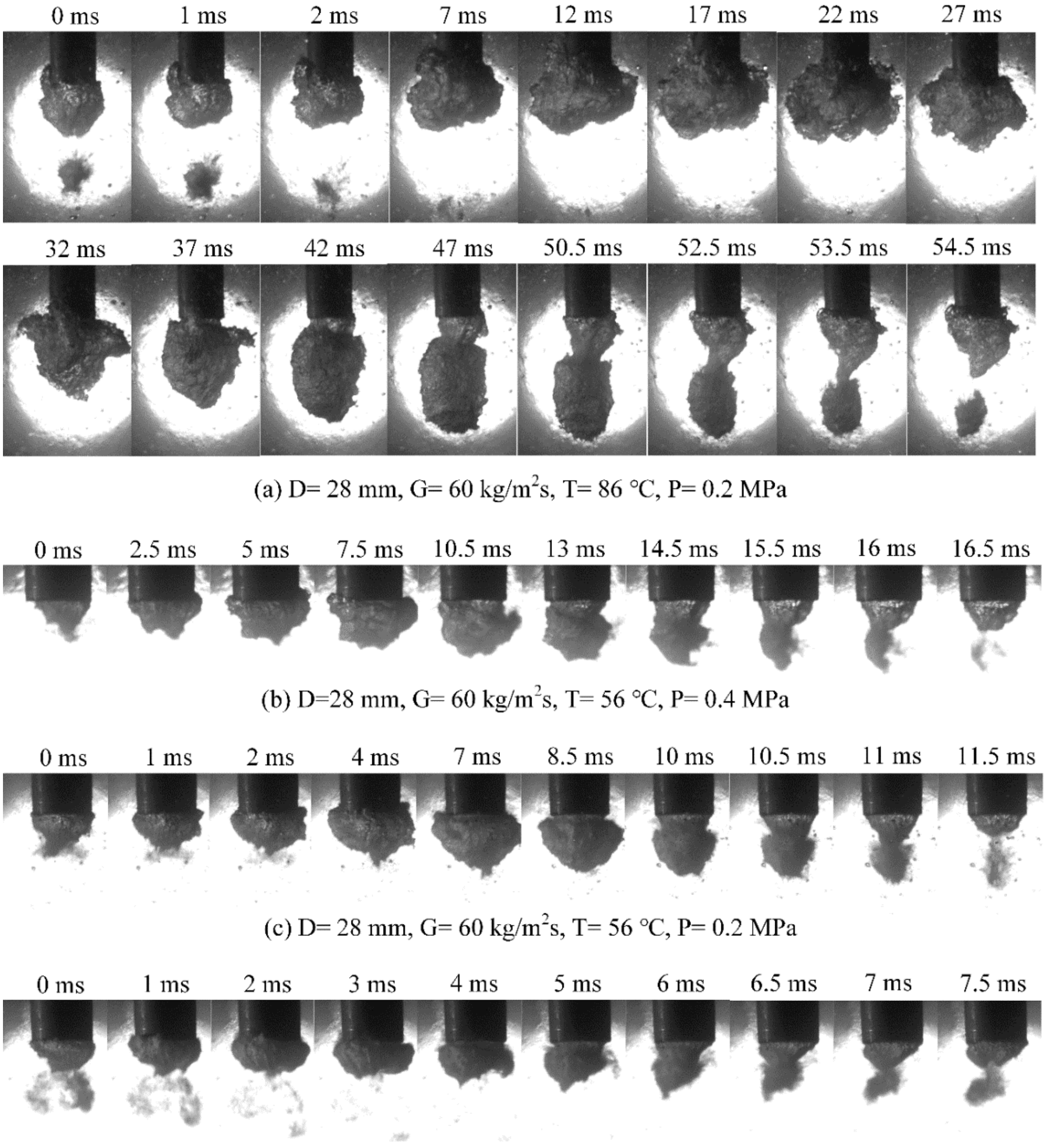

Fig. 3.8 Interface evolutions of periodic condensation oscillation

In the experiment, in addition to the continuous strong condensation oscillation as shown in Fig. 3.9, it is also found that there is an alternating condensation oscillation of strong and weak under certain experimental conditions. As shown in Fig. 3.10, although the time interval between the two adjacent "necking" processes is between 9 ms and 13.5 ms, which is highly periodic, but the maximum volume of the bubble alternates between one large and one small, and the bubble with a detached tail

also alternates between one large and one smaller.

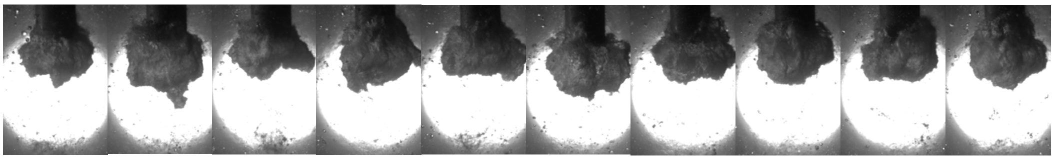

(a) The maximum volume of bubble

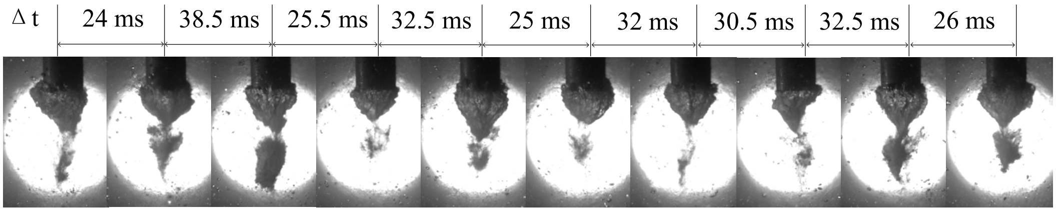

(b) The time interval between the condensation oscillation

Fig. 3.9 The images of the occurrence of periodic condensation oscillation [D = 28 mm, G = 50 kg/(m^2·s), T = 72 °C, P = 0.1 MPa]

The dynamic pressure changes in the pool and in the nozzle measured under the periodic condensation oscillation flow pattern are shown in Fig. 3.11, and the time interval between the two adjacent dynamic pressure pulse peaks is relatively consistent, which reflects the main characteristics of the periodic condensation oscillation flow pattern. Comparing the dynamic pressure curves under different experimental parameters in Fig. 3.11, it can be seen that with the increase of water temperature, the condensation rate decreases, the number of pressure pulse peaks decreases in the same time, and the pressure oscillation frequency decreases. When the steam mass flow velocity increases from 60 kg/(m^2·s) to 90 kg/(m^2·s), the pressure oscillation frequency increases, and the peak pressure pulse also increases. Unlike the effect of the steam mass flow velocity on the pressure oscillation, the pressure oscillation frequency decreases when the back pressure increases from 0.2 MPa to 0.4 MPa.

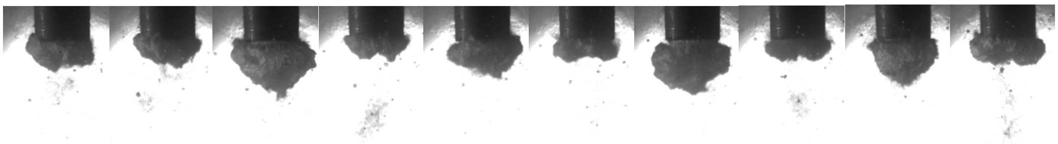

(a) The maximum volume of bubble

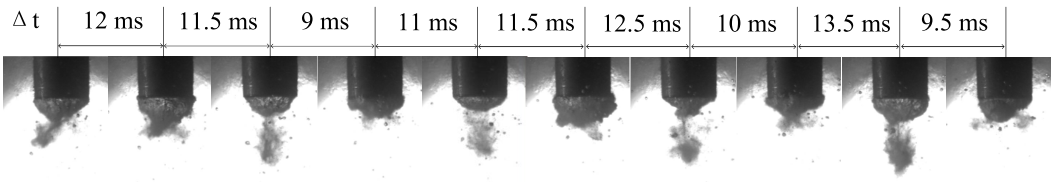

(b) The time interval between the condensation oscillation

Fig. 3.10 The images of the occurrence of periodic condensation oscillation [D = 28 mm, G = 60 kg/(m^2·s), T = 56 °C, P = 0.2 MPa]

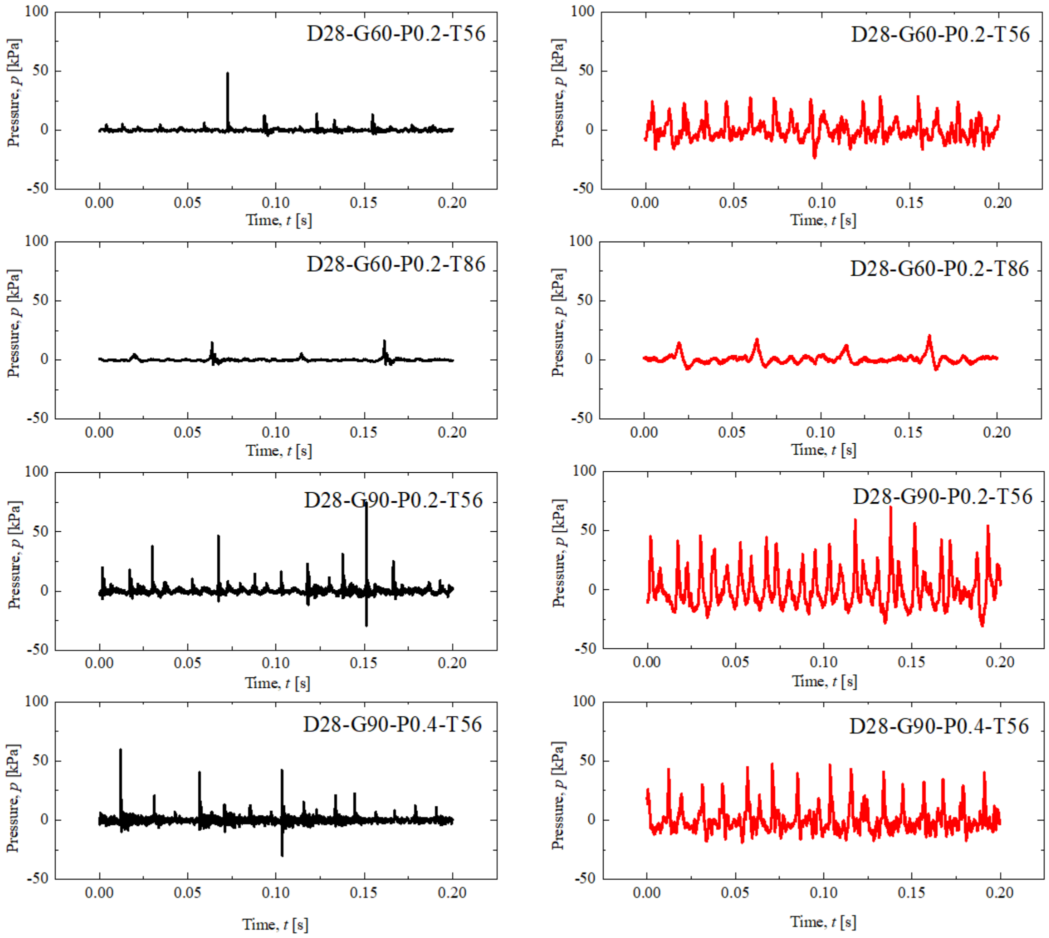

(a) Dynamic pressure in the pool

(b) Dynamic pressure in the nozzle

Fig. 3.11 Dynamic pressure of periodic condensation oscillation

3.2.4 Bubbling condensation flow pattern

When the water temperature rises above about 80 °C, the condensation flow pattern changes to bubbling condensation. At this time, the condensation capacity of the pool water is further weakened, and the steam forms a large bubble at the nozzle, and the "necking" phenomenon in the condensation oscillation flow pattern no longer appears. As shown in Fig. 3.12, there is only a slight fluctuation at the vapor-liquid interface, and the bubble as a whole sway around the nozzle outlet and break up along the outer wall of the nozzle into small bubbles, some of which are condensed by the pool water and the other part escapes from the water. After entering the bubbling condensation flow pattern, the sound generated by the bubble oscillation almost disappears, which is obviously different from the chugging flow pattern and the condensation oscillation flow pattern.

When bubbling condensation occurs, the vapor-liquid interface only fluctuates in a slight amplitude, and the whole condensation process is relatively gentle, and the resulting pressure value is also low. As shown in Fig. 3.13, the amplitude of the pressure fluctuations measured in the pool and in the nozzle is within ±4 kPa without pressure pulsation.

Between the condensation oscillation flow pattern and the bubbling condensation flow pattern, there is a flow pattern transition zone with a temperature range of about 2~8 °C. As shown in Fig. 3.14, condensation oscillation and bubbling condensation alternate in this area, and the noise generated by condensation can be heard increasing and decreasing during the experiment. Therefore, as shown in Fig. 3.15, the measured dynamic pressure changes are often characterized by a combination of pressure pulse peaks due to condensation oscillation and relatively gentle pressure fluctuations caused by bubbling condensation.

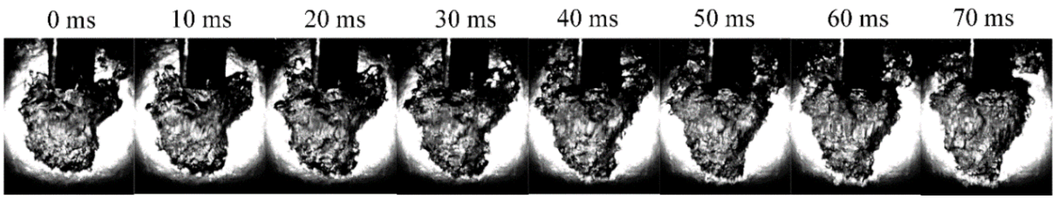

Fig. 3.12 Interface evolutions of bubbling condensation [D = 28 mm, G = 40 kg/(m^2·s), T = 80 °C, P = 0.4 MPa]

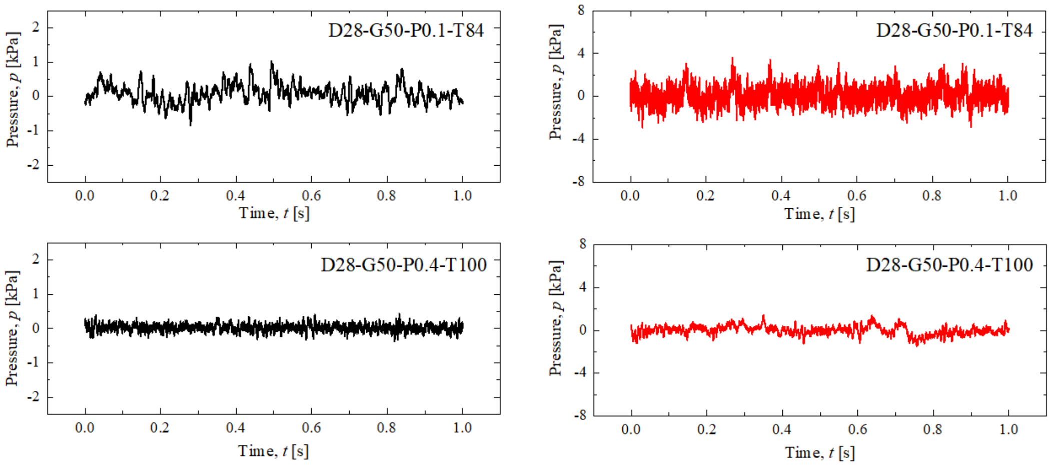

(a) Dynamic pressure in the pool (b) Dynamic pressure in the nozzle

Fig. 3.13 Dynamic pressure of bubbling condensation

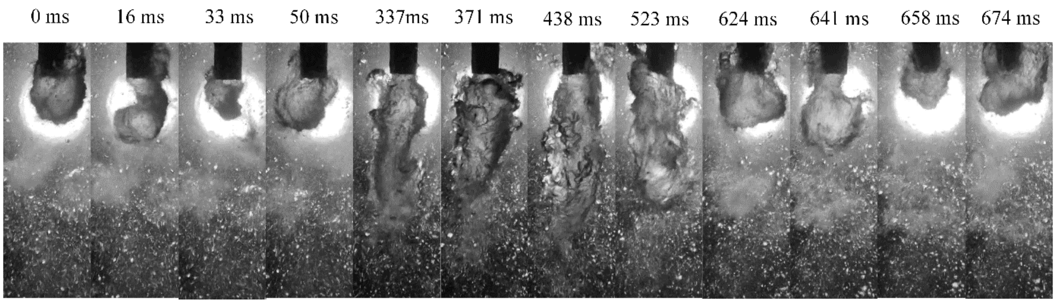

Fig. 3.14 Interface evolutions of transitional bubbling condensation [D = 28 mm, G = 50 kg/(m^2·s), T = 80 °C, P = 0.1 MPa]

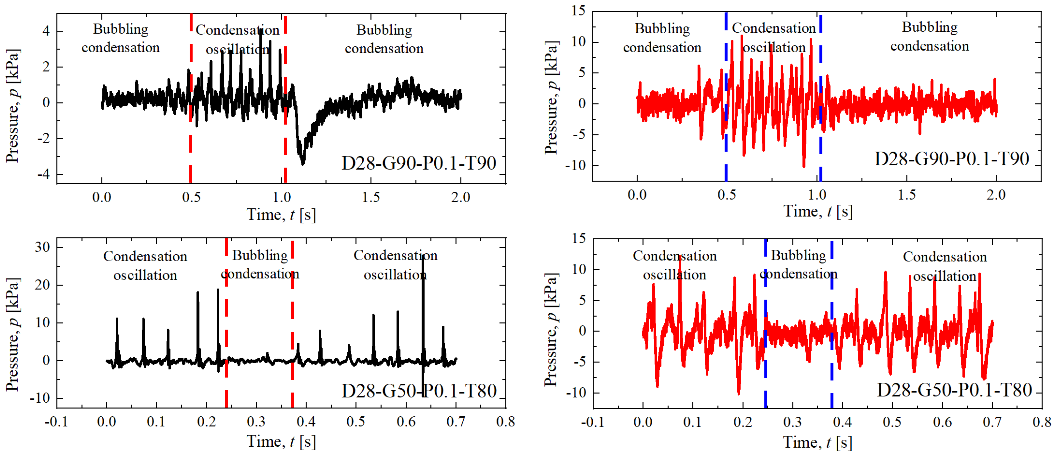

(a) Dynamic pressure in the pool (b) Dynamic pressure in the nozzle

Fig. 3.15 Dynamic pressure of transitional bubbling condensation

3.3 Jet condensation pattern boundary

3.3.1 Chugging flow pattern boundary

Fig. 3.16 illustrates the chugging flow pattern boundaries under different steam mass flow velocities, water temperatures, and back pressures. With the increase of the steam mass flow velocity, the water temperature corresponding to the chugging flow pattern boundary decreases, and the rate of decline is getting faster and faster. Among them, the boundary of the chugging flow pattern obtained in this experiment at atmospheric pressure is consistent with the change trend of the experimental results of Lahey and Moody [26] at the same back pressure (0.1 MPa). However, due to some differences in the geometric size of the nozzle selected in this experiment and Lahey and Moody's experiments, as well as the flow pattern judgment criteria, there are still some differences between the upper boundary curve of the chugging flow pattern in this experiment and that of Lahey and Moody. Compared with the experimental results under different back pressure conditions, the chugging flow pattern boundary is expanded to the direction of higher steam mass flow velocity with the increase of back pressure. For example, at atmospheric pressure, the chugging flow pattern does not occur when the steam mass flow velocity is higher than 30 kg/(m^2·s), but when the back pressure is increased to 0.4 MPa, the chugging phenomenon can be observed at lower water temperatures, even when the steam mass flow velocity is as high as 70 kg/(m^2·s).

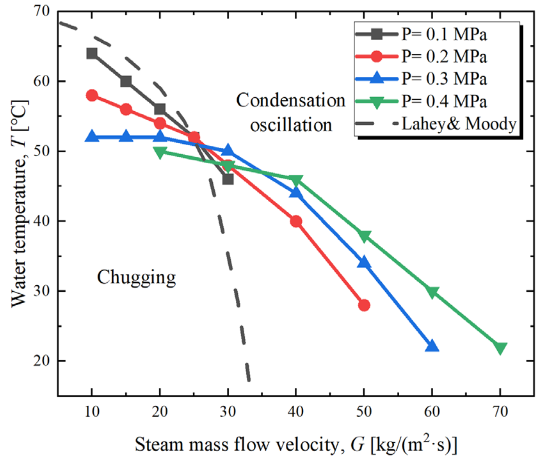

Fig. 3.16 Effect of bake pressure on chugging regime boundary (D = 28 mm)

The comparison of the chugging flow pattern boundary is obtained under the condition that the nozzle diameters are 28 mm and 38 mm, respectively. As can be seen from Figure 3.17, the larger the nozzle diameter, the larger the area occupied by the chugging flow pattern in the flow pattern, which means that chugging can still occur at higher steam mass flow velocities and water temperatures.

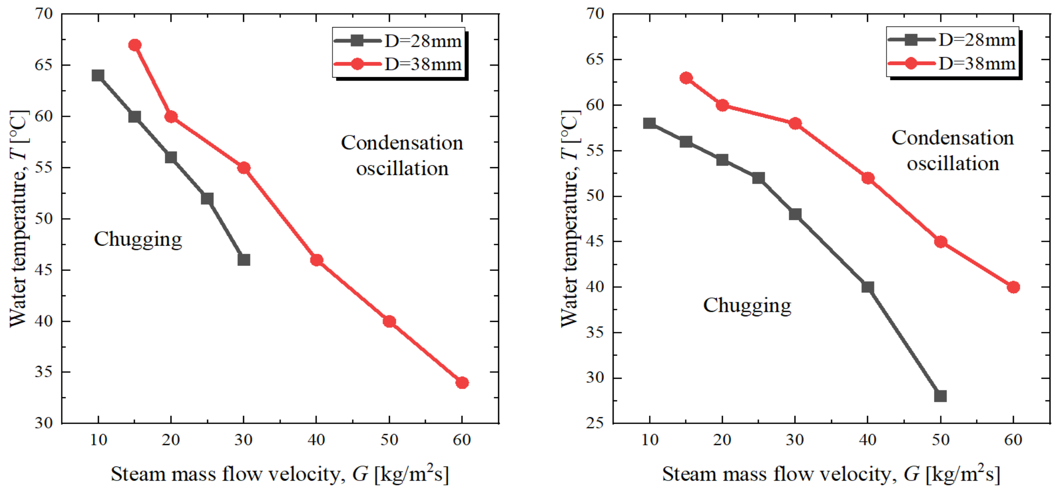

(a) P= 0.1 MPa (b) P= 0.2 MPa

Fig. 3.17 Effect of nozzle diameter on chugging regime boundary

The chugging phenomenon occurs because the condensation rate of the steam is greater than the steam flow at the nozzle outlet under the conditions of low steam mass flow velocity and high pool supercooling. Accordingly, it can be considered that when the upstream steam supply rate of the nozzle and the steam condensation rate of the nozzle are balanced, they are at the boundary of the chugging

flow pattern. According to the conservation of mass and energy:

$$\rho_s u_s A_i h_{fg} = h A_{\text{interface}} \Delta T \tag{3-1}$$

where ρ_s is the steam density, kg/m3; u_s is the steam flow rate, m/s; A_i is the cross-sectional area of the nozzle, m^2; h_{fg} is the latent heat of vaporization, kJ/kg; h is the condensation heat transfer coefficient of the vapor-liquid interface, kW/(m^2·K); $A_{interface}$ is the area of the vapor-liquid interface, m^2; ΔT is the degree of supercooling of pool water, °C.

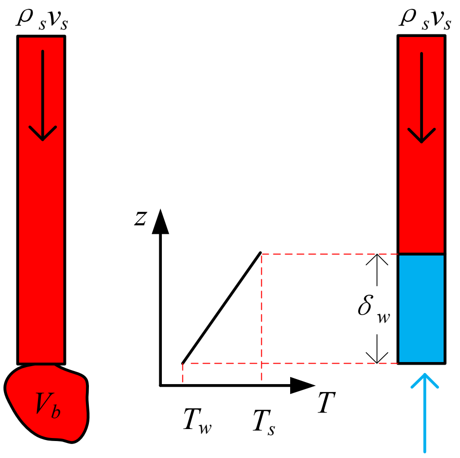

Fig. 3.18 Schematic diagram of the vapor-liquid interface when chugging occurs

Suppose that all the heat released by the bubble after condensation in the nozzle is used to heat the water column with a height of δ_w entering the nozzle. And as shown in Fig. 3.18, it is assumed that the water temperature of the water column is linearly distributed along the height of the water column. According to conservation of energy:

$$\rho_s V_b h_{fg} = 0.5 A_i \delta_w \rho_w c_p \Delta T \tag{3-2}$$

where V_b is the volume of bubble, m^3; c_p is the specific heat capacity of water, kJ/(kg·°C); ρ_w is the density of water, kg/m^3.

The formula for δ_w of the height of the water column is obtained from Eq. (3-2):

$$\delta_w = \frac{2\rho_s h_{fg} V_b}{\rho_w c_p \Delta T A_i} \tag{3-3}$$

According to the assumptions of Liang and Griffith's [14] transient thermal conductivity model, a layer of warm water will be formed at the interface periodically during the expansion and contraction of the vapor-liquid interface, and the condensation heat transfer coefficient h of the interface can be estimated by the following formula:

$$h = \frac{\lambda}{\delta_w} \tag{3-4}$$

where λ is the thermal conductivity of water, W/(m·K).

Because it is at the boundary of the chugging flow pattern, the vapor-liquid interface is in a critical state when it is about to enter the nozzle, so the area of the vapor-liquid interface $A_{interface}$ is approximately equal to the cross-sectional area of the nozzle.

$$A_{\text{interface}} \approx A_i = \frac{\pi D^2}{4} \tag{3-5}$$

where D is the inner diameter of the nozzle, m.

Assuming that the volume of the bubble and the diameter of the nozzle conform to the following form:

$$V_b = cD^3 \tag{3-6}$$

Simultaneous equations (3-1), (3-3), (3-4), (3-5) and (3-6), the following relationship is obtained,

$$k Re_w^{s\,0.5} Pr^{0.5} Ja^{-1} = 1 \tag{3-7}$$

Thereinto:

$$Re_w^s = \frac{\rho_w u_s D}{\mu_w} \tag{3-8}$$

$$Pr = \frac{\mu_w c_p}{\lambda} \tag{3-9}$$

$$Ja = \frac{\rho_w c_p \Delta T}{\rho_s h_{fg}} \tag{3-10}$$

Considering the difference between the assumption of the bubble volume and the actual situation and the effect of back pressure on the boundary of the chugging flow pattern, the back pressure correction term is added to Eq. (3-7). Then, the experimental datas are used to fit the coefficients of Eq. (3-7) and the exponential term of the interface

Reynolds number. Finally, the formula for determining the upper boundary of the chugging flow pattern shown in Eq. (3-11) is obtained.

$$40.37 Re_w^{s\,0.041} Pr^{0.5} Ja^{-1} (P/P_0)^{-0.322} \le 1 \tag{3-11}$$

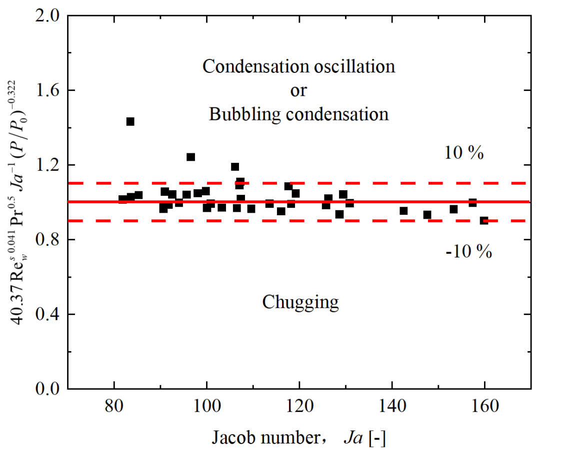

Fig. 3.19 Criterion for chugging regime boundary

That is, if the parameters meet the conditions of Eq. (3-11), the condensation flow pattern is in the chugging region, otherwise it is condensation oscillation or bubbling condensation and other flow patterns. As can be seen from Figure 3.19, for more than 90% of the experimental data points located on the boundary between chugging and condensation oscillation, the judgment error of Eq. (3-11) is within ±10%.

3.3.2 Periodic condensation oscillation flow pattern boundary

Fig. 3.20 shows the upper and lower boundaries of the periodic condensation oscillation flow pattern under different back pressure conditions, and it can be seen that the area occupied by the periodic condensation oscillation in the flow pattern diagram gradually decreases with the increase of back pressure under the two nozzle diameter conditions, especially the lower boundary of the periodic condensation oscillation flow pattern. This is because chugging and non-periodic condensation oscillation can occur at higher water temperatures as the back pressure increases.

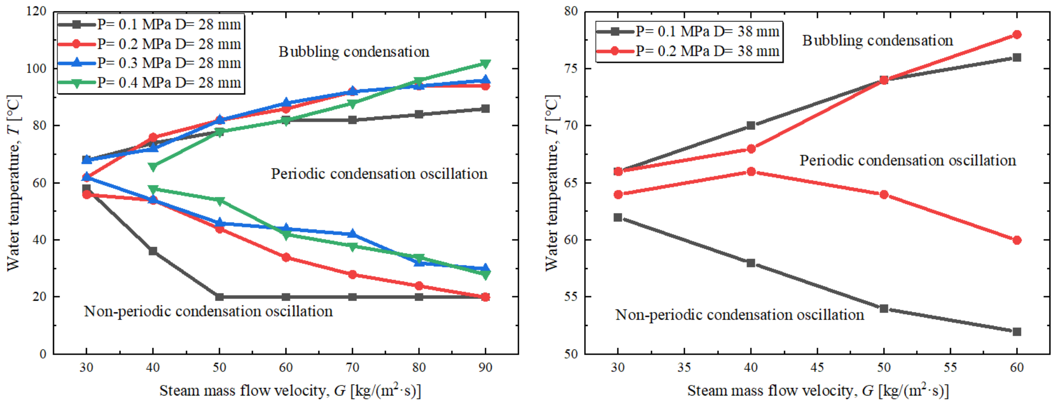

(a) D=28mm (b) D=38mm

Fig. 3.20 Effect of bake pressure on periodic condensation oscillation regime boundary

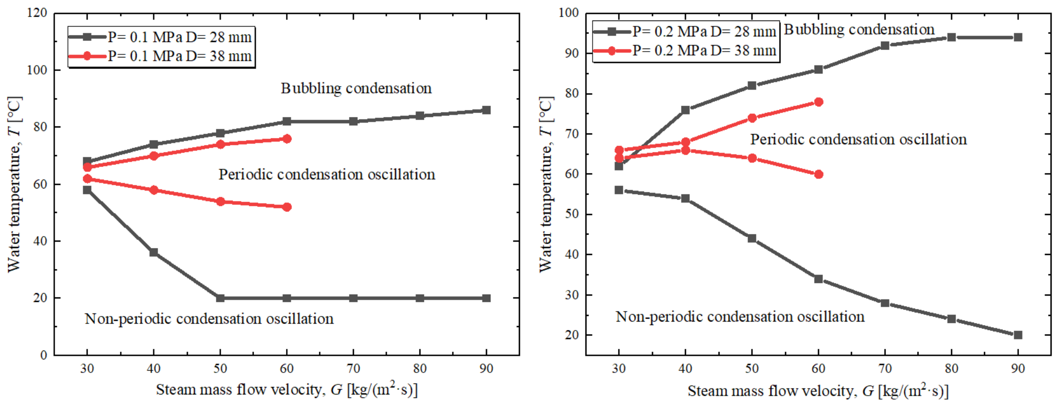

(a) P=0.1MPa (b) P=0.2MPa

Fig. 3.21 Effect of nozzle diameter on periodic condensation oscillation regime boundary

Fig. 3.21 shows the upper and lower boundaries of the periodic condensation oscillation flow pattern under different nozzle diameters, similar to the effect of back pressure, the larger the nozzle diameter, the more likely it is to chugging, and the condensation process tends to be unstable, making it difficult to form periodic condensation oscillation, so the range of periodic condensation oscillation also decreases with the increase of nozzle diameter.

3.3.3 Boundary of bubbling condensation flow pattern

Fig. 3.22 and Fig. 3.23 show that in the low steam flow velocity region, the bubbling condensation generally starts between the water temperature reaches 70~80 °C, and the water temperature at the lower boundary of the bubble flow pattern increases gradually with the increase of the steam mass flow velocity, but the back pressure and nozzle diameter have no obvious influence on the water temperature of the flow pattern transition.

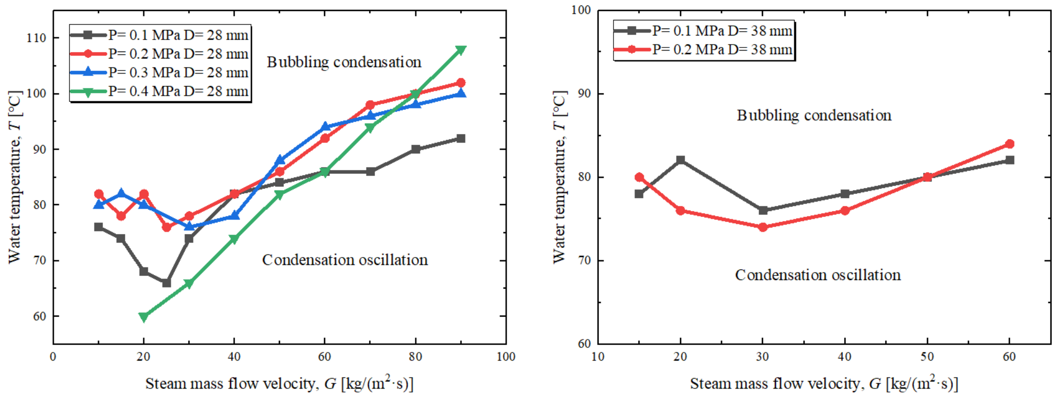

(a) D=28mm (b) D=38mm

Fig. 3.22 Effect of bake pressure on bubbling condensation regime boundary

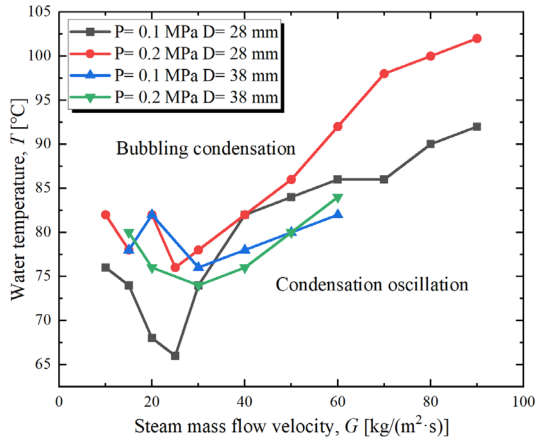

Fig. 3.23 Effect of nozzle diameter on bubbling condensation regime boundary

4. CONCLUSIONS

Based on the steam jet condensation experimental setup, the study of steam jet condensation patterns under different back pressures is carried out, and the phase interface characteristics and dynamic pressure characteristics of different condensation patterns are mainly compared and analyzed, and the boundaries between different condensation patterns are summarized, and the main conclusions are as follows:

(1) Under different back pressure conditions and different nozzle diameters, the condensation patterns of steam jet are established, which mainly include four condensation patterns with typical phase interface and dynamic pressure characteristics, namely chugging, non-periodic condensation oscillation, periodic condensation oscillation and bubbling condensation.

(2) Under the condition of higher back pressure,

chugging is more likely to occur, and the boundary range of chugging flow pattern is broadened. The water temperature corresponding to the boundary of the chugging flow pattern decreases gradually with the increase of steam mass flow velocity, and gradually increases with the increase of nozzle diameter.

(3) Based on the principle of conservation of energy, the judgment formula of the chugging flow pattern is given, and the results show that the relative deviation between the predicted value and the measured value of more than 90% in the experiment is within ±10%.

(4) With the increase of back pressure and nozzle diameter, the boundary range of periodic condensation oscillation flow pattern decreases, but the influence of back pressure and nozzle diameter on the boundary of bubbling condensation flow pattern is not obvious.

References

[1] Yong C, Hong G, Hanzhou L, et al. Experimental investigation on condensation regimes and transition boundary during bubble condensation in narrow rectangular channel[J]. International Journal of Thermal Sciences,2023,188

[2] Abdul Q, Ajmal S, Rasheed K Q, et al. Study of steam jet characteristics and regime maps for bevelled spray nozzles exhausting into quiescent water[J]. International Journal of Heat and Mass Transfer,2022,190

[3] Du Y, Yan X, Zang J, et al. Review of Regime Maps of Steam-Submerged Direct Contact Condensation[J]. Frontiers in Energy Research,2020,8119.

[4] Xiao J, Hrnjak P. A flow regime map for condensation in macro and micro tubes with non-equilibrium effects taken into account[J]. International Journal of Heat and Mass Transfer,2019,130893-900.

[5] Li W, Wang J, Zhou Y, et al. Investigation on steam contact condensation injected vertically at low mass flux: Part I pure steam experiment[J]. International Journal of Heat and Mass Transfer,2019,131301-312.

[6] Weichao L, Zhaoming M, Zhongning S, et al. Investigation on steam direct contact condensation injected vertically at low mass flux, part II: Steam–air mixture experiment[J]. International Journal of Heat and Mass Transfer,2020,155.

[7] Arinobu M. Studies on the dynamic phenomena caused by steam condensation in water[C]//Proc. of ANS-ASME-NRC Int. Topical Meeting on Nuclear Reactor Thermal Hydraulics: Vol. 1. 1980: 293-302.

[8] Chan C K, Lee C K B. A regime map for direct contact condensation[J]. International Journal of Multiphase Flow, 1982, 8(1): 11-20.

[9] Nariai H, Aya I. Fluid and pressure oscillations occuring at direct contact condensation of steam flow with cold water[J]. Nuclear Engineering and Design, 1986, 95(C): 35-45.

[10] Cho S, Song C H, Park C K, et al. Experimental study on dynamic pressure pulse in direct contact condensation of steam jets discharging into subcooled water[C]//Proceedings of NTHAS98. Pusan, Korea: KNS, 1998: 529.

[11] Mazed D, Lo Frano R, Aquaro D, et al. Experimental investigation of steam condensation in water tank at sub- atmospheric pressure[J]. Nuclear Engineering and Design, 2018, 335: 241-254.

[12] Lee S I, No H C. Gravity-driven injection experiments and direct-contact condensation regime map for passive high-pressure injection system[J]. Nuclear Engineering and Design, 1998, 183(3): 213-234.

[13] Zhao Q, Hibiki T. Review: Condensation regime maps of steam submerged jet condensation[J]. Progress in Nuclear Energy, 2018, 107: 31-47.

[14] Liang K S, Peter-Griffith. Experimental and analytical study of direct contact condensation of steam in water[J]. Nuclear Engineering and Design, 1994, 147(3): 425-435.

[15] Xiao J, Hrnjak P. A flow regime map for condensation in macro and micro tubes with non-equilibrium effects taken into account[J].

International Journal of Heat and Mass Transfer,2019,130893-900.

[16] Xiao J, Hrnjak P. A new flow regime map and void fraction model based on the flow characterization of condensation[J]. International Journal of Heat and Mass Transfer,2017,108443-452.

[17] Afzal H, Shah A, Quddus A, et al. Experimental study on effect of submergence depth on steam jet shape characteristics in direct contact condensation[J]. Chemical Engineering Research and Design,2024,207243-256.

[18] Aoyue H, Qiang X, Shuaizhi J, et al. Experimental study of interface behavior and sound pressure oscillation of direct contact condensation of a steam jet in flowing water[J]. Experimental Thermal and Fluid Science,2024,150

[19] Qiang X, Chenying L, Qimeng L, et al. Interfacial characteristics of steam jet condensation in subcooled water pipe flow–An experimental and numerical study[J]. Chemical Engineering Science, 2022,251

[20] Xu Q, Liu W, Li W, et al. Experimental investigation on interfacial behavior and its associated pressure oscillation in steam jet condensation in subcooled water flow[J]. International Journal of Heat and Mass Transfer,2019,145118779-118779.

[21] Xinxing L, Mingrui Y, Wei L, et al. Characteristics of fluid and pressure oscillations induced by steam injected through a vertical blow down pipe under different vessel pressures[J]. Annals of Nuclear Energy,2022,173.

[22] Xinxing L, Mingrui Y, Wei L, et al. Experimental investigation of the pressure oscillations induced by subsonic steam jets under different vessel pressures[J]. Nuclear Engineering and Design,2022,395.

[23] Xinxing L, Xiangjie Q, Nan Z, et al. Scaling analysis of the pressure suppression containment test facility for the small pressurized water reactor[J]. Nuclear Engineering and Technology,2020,53(3):793-803.

[24] Chong D, Liu W, Zhao Q, et al. Oscillation characteristics of periodic condensation induced water hammer with steam discharged through a horizontal pipe[J]. International Journal of Heat and Mass Transfer, 2021, 173: 121265.

[25] Sun J, Lu C, Mi Z, et al. Experimental research on characteristics of condensation induced water hammer in natural circulation systems[J]. International Communications in Heat and Mass Transfer, 2020, 114: 104559.

[26] Lahey R T, Moody F J. The thermal-hydraulics of a boiling water nuclear reactor[M]. 2nd ed. La Grange Park, Ill., USA: American Nuclear Society, 1993.